lncRNA *NORM* is essential for proper chromosome segregation through the Plk1-Bub1 and Nsun2 axis.

Vikas Dongardive[1], Sonali Jathar[1], Juhi Srivastava[1] and Vidisha Tripathi[1*]

[1]Laboratory of lncRNA Biology, National Centre for Cell Science, NCCS Complex, Savitribai Phule Pune University Road, Pune-411007, MH, INDIA

*Address correspondence to: Vidisha Tripathi (tvidisha@nccs.res.in)

Running Title: NORM coordinate Plk1-Bub1-Nsun2 in chromosome segregation

Abbreviations: BrdU-5-bromo-2'-deoxyuridine ; CDK-Cyclin Dependent Kinase ; CPAT-Coding Potential Assessment Tool ,CPC-Coding Potential Calculator ; FACS-Fluorescence-activated single cell sorting ; KT-Kinetochore; LNA-ASO -Locked nucleic acid- anti sense oligonucleotide; lncRNA-Long noncoding RNA ;MT-Microtubule; Nsun2-NOP2/Sun RNA methyltransferase 2; Plk1-Polo-like kinase 1; RIP-RNA immunoprecipitation ; SAC -Spindle assembly checkpoint ;SCR-Scramble

Abstract:

The cell cycle comprises different phases and is a tightly regulated process at the molecular level. During the cell cycle, two key events occurred: DNA duplication during the S phase and chromosome segregation during mitosis. Accurate cell cycle progression, achieved through faithful chromosome segregation, is essential for maintaining cell fidelity. Long noncoding RNAs are a subclass of noncoding RNA that are longer than 200 bp and form RNA protein complexes (RNPs) to regulate various biological processes. Herein, we demonstrate that lncRNA *NORM* is involved in regulating the cell cycle by maintaining proper chromosome segregation. *NORM* exhibited G2 phase-specific expression, and the depletion of *NORM* resulted in a significant G2/M arrest. *NORM*-depleted cells failed to progress in mitosis and showed defects in chromosome segregation. We further demonstrated that *NORM* binds to proteins such as Plk1 and Nsun2. Depletion of *NORM* hindered the interaction between Plk1 and Bub1, resulting in reduced kinetochore localization of Plk1 during prometaphase. Our results also show that the depletion of *NORM* affects the binding of Nsun2 protein to CDK1 mRNA and, consequently, the stabilization of CDK1 at the protein level. Altogether, our results demonstrate that *NORM* regulates chromosome segregation by mediating the interaction between Plk1 and Bub1.

Keywords: long noncoding RNA, cell cycle, chromosome segregation, Plk1, Bub1, Mitosis.

Introduction:

The mammalian cell cycle is a ubiquitous and tightly regulated process that comprises events orchestrated in an orderly manner to culminate in the formation of two daughter cells. The entry of a cell into different phases of the cell cycle is precisely controlled by the oscillating concentrations of different Cyclins and CDK complexes. In addition to Cyclins and CDKs, various cyclin kinase inhibitors (CKIs) and cell cycle regulatory proteins, such as RB, p53, and p21, regulate the cell cycle (1,2). Two key events that occur during the cell cycle are the duplication of genetic material in the S phase and the segregation of chromosomes in the M phase. Precise control of chromosome segregation during the M phase is crucial for error-free cell cycle progression, as any defect in chromosome segregation can lead to cellular abnormalities that ultimately contribute to the development of various cellular disorders, including cancer (3). One of the key events that is responsible for faithful chromosome segregation is the attachment of the kinetochore to microtubules (KT-MT) (4). A plethora of proteins are involved in mediating the proper attachment of KT-MT for the segregation of chromosomes. Any defect in chromosome segregation is detected by the surveillance mechanism known as the spindle assembly checkpoint (SAC), which is activated to correct the erroneous microtubule-to-kinetochore attachment (5). Budding uninhibited by benzimidazoles 1 (Bub1) plays a pivotal role in assembling the SAC complex by localizing at the kinetochore through the phosphorylation of Knl1 by Mps (6,7). Phosphorylated Knl1 then recruits the Bub3-Bub1 complex. Additionally, Mps1 phosphorylates Bub1 to mediate its interaction with the Mad1-Mad2 complex, thereby creating a SAC signaling platform (8). This platform then further recruits Bub3, BubR1, Cdc20, and Mad2. Bub1 also binds to another kinase, Polo-like kinase 1 (Plk1), and the interaction between Plk1 and Bub1 is essential for the kinetochore localization of Plk1. Any defects in Plk1 kinetochore localization cause chromosome mis-segregation, marked by chromosomes associated with spindle poles (9). The interaction between Bub1 and Plk1 primarily depends on Bub1's phosphorylation at T609, mediated by the CDK1 protein (9). The Cyclin B and CDK1 complex drives the entry of a cell into mitosis and is crucial for guaranteeing accurate and faithful segregation of duplicated chromosomes. CDK1 is also regulated by various proteins, such as MYT1 and WEE1, which deactivate CDK1 through phosphorylation (10,11). Moreover, CDK1 is also regulated through mRNA stabilization by the protein binding to its mRNA. NOP2/Sun RNA methyltransferase family, member 2 (NSun2) (Misu) stabilizes CDK1 and enhances its translation by binding to its mRNA and methylating its 3' untranslated region (UTR) (12). CDK1 binds to Cyclin B and becomes activated. Upon activation, it phosphorylates various substrates, including Bub1, which is crucial for mitosis and contributes to the faithful segregation of chromosomes. Multiple lines of evidence suggest that noncoding RNAs, including microRNAs (miRNAs) and long

97 noncoding RNAs (lncRNAs), are also involved in regulating the cell cycle. lncRNAs are a class
98 of noncoding RNAs that are longer than 200 bp and characterized by their short open reading
99 frame. By forming RNP complexes, lncRNAs are known to control a variety of biological
100 processes through Signal, decoy, Guide, or Scaffold mechanisms. In a recent study, it has
101 been demonstrated that lncRNA MALAT1 is differentially regulated during the G1/S and M
102 phases and is essential for the progression of the cell cycle from G1/S to S and from G2 to M,
103 through the transcription and alternative splicing of the gene bMyb (13). Another study has
104 demonstrated that the lncRNA EMS controls the cell cycle progression during the G1/S phase.
105 EMS stabilizes E2F1 mRNA by binding to the RALLY protein in a manner that increases the
106 expression of that gene (14). lncRNAs also interact with CDKs to regulate cell cycle
107 progression. A recent study revealed that lncRNA HOXC-AS3 interacts with CDK2, thereby
108 facilitating reduced binding of CDK2 to p21, which ultimately leads to increased CDK2 activity
109 and promotes cell proliferation (15). Several other studies have demonstrated that many long
110 noncoding RNAs (lncRNAs) play a role in cell cycle regulation. Among these lncRNAs,
111 LINC00667 is an interesting lncRNA due to its recently studied role in multiple diseases,
112 specifically in cancers and chronic kidney diseases. Recently, various studies have shown
113 that LINC00667 is differentially expressed in various cancer cell lines and plays a crucial role
114 in regulating cellular proliferation, invasion, migration, and apoptosis (16–19).Overexpression
115 of LINC00667 in renal tubular epithelial cells results in chronic renal fibrosis by increasing
116 cellular proliferation, migration, and apoptosis through the miR-19b-3p/LINC00667/CTGF
117 axis(16). Upregulation of LINC00667 in clear renal carcinoma is associated with increased
118 cellular proliferation, migration, and invasion, achieved through the targeting of miR-143-3p
119 and a subsequent increase in ZEB1 expression (20). Furthermore, LINC00667 also plays an
120 oncogenic role in various cancers, including Wilms' tumor, through the miR-200b/c/429 and
121 IKK-β axis (18). In non-small cell lung cancer, it plays its role via EIF4A3-stabilized
122 VEGFA(17). In breast cancer, LINC00667 drives tumor growth and chemoresistance to
123 docetaxel through the miR-200/Bcl2 axis (21). Additional evidence suggests that LINC006677
124 is upregulated in nasopharyngeal carcinoma, enhancing proliferation, migration, and the
125 epithelial-to-mesenchymal transition by sponging miR-4319 and regulating the level of FOXQ1
126 (22). In esophageal cancer, LINC00667 is associated with promoting proliferation through the
127 LINC00667/miR-200b-3p/SLC2A3 axis(23). In cholangiocarcinoma, LINC00667 regulates
128 tumor growth through YY1-mediated upregulation (24). Together, these findings highlight
129 LINC00667 as a crucial molecular regulator of proliferation in cancer and kidney disease,
130 underscoring the need for further investigation to elucidate its mechanisms and therapeutic
131 potential. Its consistent involvement in regulating cellular proliferation hints at a broader role
132 in cell cycle control, an area that remains largely unexplored. Understanding this potential
133 connection may uncover new therapeutic avenues for diseases where aberrant cell cycle

regulation is a hallmark. Understanding the involvement of lncRNAs in cell cycle regulation will provide a detailed molecular mechanism and open up new opportunities for novel treatments of cellular disorders associated with cell cycle dysregulation.

In this study, we showed the involvement of LINC00667 in regulating the cell cycle. We demonstrated that long noncoding RNA LINC00667 is crucial for proper chromosomal segregation by modulating the interaction between Plk1 and Bub1. LINC00667 is a G2-phase enriched lncRNA and is essential for driving the G2/M progression of the cell. LINC00667 depletion causes G2/M arrest of cells marked with chromosome misalignment, which ultimately results in cell apoptosis. The interaction between Plk1 and Bub1 is hampered upon LINC00667 depletion. We have demonstrated the molecular relationship between LINC00667 and another protein, Nsun2. Additionally, we have demonstrated that LINC00667 depletion reduces the binding of Nsun2 to CDK1 mRNA, thereby decreasing the stability of the CDK1 protein. We observed that a reduced level of CDK1 protein results in a decrease in the phosphorylation of Bub1 at T609. Finally, Plk1 localization at the kinetochore is altered as a result of hindering the interaction between Plk1 and Bub1. Overall, our research suggests that the novel long non-coding RNA (lncRNA) LINC00667 plays a crucial role in regulating the cell cycle by ensuring normal chromosome segregation.

Results:

NORM is upregulated during the G2 phase of the cell cycle and promotes G2/M transition

Tumour cells adapt pathways that bypass normal cell cycle checkpoints to enable unregulated cell division. Uncontrolled proliferation is often driven by signalling pathways that alter the expression of cell cycle regulators such as cyclins, cyclin-dependent kinases (CDKs), and CDK inhibitors. Therefore, oncogenic lncRNAs such as LINC00667, which promote proliferation, may exert their function at least in part by regulating cell cycle processes. Recent studies have demonstrated that one such long non-coding RNA (lncRNA), LINC00667, is differentially regulated in various cancers and plays a role in regulating proliferation. Uncontrolled cellular proliferation is one of the hallmarks of cancer, often resulting from defects in the cell cycle regulation program. The cell cycle is a more complex phenomenon that is coordinated through multiple layers of regulation, driven by proteins as well as a wide array of noncoding RNAs, including long noncoding RNAs (lncRNAs) and microRNAs (miRNAs). One of our comprehensive studies has identified a set of cell cycle-related long noncoding RNAs (lncRNAs), with most of these lncRNAs exhibiting cell cycle phase-specific expression patterns. LINC00667 is one such lncRNA that showed G2 phase-specific expression in

169 synchronized HeLa cells. Based on its function, we named LINC00667 the Noncoding RNA
170 Regulator of Mitosis *(NORM). NORM* is approx. 4.0 nucleotides long noncoding transcript
171 located on chromosome 18 (chr18:5,232,875-5,290,608 (GRCh38/hg38)), Histone tail
172 modification map indicated a significant H3K4me3 and H3K27ac marks on the promoter of
173 *NORM*, indicating that it is actively transcribed across different cell types **[FIG 1A].** The coding
174 probability of the *NORM* transcript was analyzed using the CPAT tool, revealing that *NORM*
175 does not code for any protein, unlike the well-characterized long noncoding RNA MALAT1
176 **[FIG. 1B].** To understand its cis-acting or trans-acting mode, *NORM* was further characterized
177 for its subcellular localization using a subcellular fractionation method, followed by a
178 quantitative real-time PCR analysis to assess the level of *NORM*. Quantitative real-time PCR
179 data revealed that *NORM* is predominantly located in the nucleus, with some fraction also
180 present in the cytoplasm **[FIG. 1C].** Quantitative real-time PCR (qRT-PCR) analysis revealed
181 that the transcript levels of *NORM* remain low during the G1 and S phases of the cell cycle.
182 However, there is a steady increase in transcript levels during the G2 phase, followed by a
183 subsequent decrease in the M phase **[FIG. 1D].** Cell cycle phase-specific expression of
184 lncRNAs is often associated with their role in that specific phase. An elevated level of *NORM*
185 in the G2 phase suggests its potential role in regulating G2/M progression. To understand
186 whether *NORM* is required for normal cell cycle progression and to examine the functional
187 relevance of *NORM*, Antisense oligonucleotide (ASO)- based depletion of *NORM* was
188 performed, followed by cell cycle analysis by using propidium iodide (PI) based fluorescence-
189 activated cell sorting (FACS), which showed a significant G2/M arrest in asynchronously
190 growing WI-38 cells **[FIG. 1E, F, and H]**. The effect of *NORM* depletion on cell cycle
191 progression was further confirmed by performing BrdU-PI flow cytometry. We observed a
192 significant increase in the G2/M population upon *NORM* depletion, confirming that *NORM*
193 depletion leads to cell cycle arrest at the G2/M phase **[FIG. G]**. It was evident from the cell
194 cycle analysis that the absence of *NORM* caused a significant G2/M arrest in the cell cycle,
195 indicating the importance of *NORM* in driving cells through the G2/M phase. We further
196 confirmed the role of *NORM* in driving G2/M progression by arresting the asynchronously
197 growing HeLa cells in mitosis with Nocodazole treatment, followed by subsequent release in
198 control and *NORM*-depleted conditions, and then analyzed by PI-FACS. PI-flow cytometry
199 analysis indicated that in the control condition, cells were correctly arrested upon nocodazole
200 treatment and subsequently progressed from the G2/M phase to the G1 phase upon release.
201 Nevertheless, in the *NORM* depletion condition, cells failed to progress from the G2/M phase
202 to the G1 phase even after 10 hours of release **[FIG. 1I & J].** Moreover, we observed that the
203 level of CDK1 was reduced upon *NORM* depletion compared to the control, as determined by
204 our immunoblot analysis **[Fig. 1K]**. This indicates the importance of *NORM* in driving the cells
205 through the G2/M phase. As DNA content-based cell cycle analysis is incapable of

206 distinguishing between the G2 and M-phase populations, we employed H3ser10
207 phosphorylation-based cell cycle analysis. A close examination of G2 and M phase
208 populations revealed that *NORM* depletion results in a substantial decrease in the mitotic
209 phase population and an increase in the G2 phase population, indicating a failure of the cells
210 to progress from the G2 to the M phase **[FIG. 1 L&M]**. This was further confirmed by
211 immunoblotting analysis, which checked the level of phospho-H3 at the ser10 residue. The
212 level of phospho-H3 (ser10) was significantly reduced upon *NORM* depletion **[FIG. 1 N]**.

213 **Loss of *NORM* affects cellular proliferation, leading to an increase in apoptosis.**

214 Depletion of *NORM* resulted in a marked increase in the G2/M population, prompting us to
215 investigate the effect of *NORM* on cellular proliferation. The effect on proliferation was
216 evaluated by performing Ki-67 immunostaining. The results showed a considerable decrease
217 in Ki-67-positive cell numbers in *NORM*-depleted conditions compared to control conditions
218 **[FIG. 2A & B]**. *NORM* depletion resulted in a substantial reduction in cellular viability and
219 proliferation, as well as a significant decrease in colony formation ability, as observed through
220 the MTT assay and clonogenic assay, respectively, confirming the observations about
221 proliferation **[FIG 2C, D, and E].** This data revealed that *NORM* depletion significantly reduced
222 cell proliferation, suggesting that *NORM* depletion can lead to defects in cell cycle progression.
223 The cell cycle analysis data showed an increase in the sub-G1 population upon *NORM*
224 depletion, indicating a significant level of apoptosis in the absence of the lncRNA. We then
225 determined the level of apoptosis in *NORM*-depleted cells by performing Annexin V-FITC and
226 propidium iodide (PI) based flow cytometry. The flow cytometry data showed an increase in
227 early and late apoptotic populations upon *NORM* depletion compared to those in control cells
228 **[FIG. 2E & F].** Increased levels of cleaved PARP in *NORM*-depleted conditions further
229 validated the result. Additionally, anti-apoptotic protein Bcl2 levels were decreased, while pro-
230 apoptotic protein Bax levels were increased upon *NORM* depletion **[FIG. 2G].** The overall data
231 suggest the importance of *NORM* in promoting cellular proliferation and inhibiting apoptosis.

232 **Loss of *NORM* results in changes in gene expression at the global transcriptomic and**
233 **proteomic levels.**

234 To understand the molecular mechanism underlying the cell cycle defect upon *NORM*
235 depletion, we analyzed gene expression changes by performing a global transcriptome
236 analysis on control and *NORM*-depleted samples using the Illumina HiSeq 2500 platform.
237 Global transcriptome profiling revealed that the loss of *NORM* results in the differential
238 expression of 1,050 genes, wherein nearly 500 genes showed more than 2.5-fold up-
239 regulation, while 550 genes showed more than 2.5-fold down-regulation **[FIG. 3A]**. ZNF48,
240 SLC16A6, BRCA1, CHRND, PCNT, DCAKD, POT1, ZNF74, RNF14, and YY1AP1 were the

241 top down-regulated genes, while SEC31A, ITGA2, FBXO6, DNM2, SMURF1, GUCD1, WDR4,
242 POP1, PPP1R7, and PSMD1 were the top up-regulated genes **[Supplementary figure 1.1]**.
243 Using qRT-PCR, we validated the expression of several differentially expressed genes
244 (DEGs), which showed a similar trend **(Supplementary 1.2).** We next analysed the effect of
245 *NORM* on cellular biological pathways by performing gene ontology analysis. Gene ontology
246 revealed that many cell cycle-related biological processes and pathways were affected by
247 *NORM* depletion. The top ten down-regulated biological processes and upregulated biological
248 processes include cell cycle-related pathways such as regulation of mitotic cell cycle phase
249 transition, regulation of cell cycle phase transition, positive regulation of cell cycle, G2/M
250 transition of the mitotic cell cycle, and cell cycle G2/M phase transition **[FIG 3B &C]**. The
251 down-regulation of G2/M transition-related genes, such as MELK, CEP70, CDK2, PPP2R2A,
252 PCNT, and CDC25A, suggests a failure in the G2/M transition in the absence of *NORM*. To
253 gain further insight, we performed a proteomics analysis in *NORM*-depleted and control
254 conditions to check the effect of *NORM* depletion on different proteins and biological
255 processes. *NORM* depletion resulted in > 2-fold down-regulation of 146 proteins and > 2-fold
256 up-regulation of 679 proteins **[FIG 3D].** Many cell cycle-related proteins showed differential
257 expressions. Proteins known for their role in cell cycle regulation, such as TGM2, PSMD,
258 CLTC, PSMD2, BUB3, and ANXA4, were significantly upregulated. In contrast, proteins such
259 as PDGFRB, PTMS, COL1A1, CD2AP, LAMB2, YWHAB, CDK1, MCM3, and YWHAG were
260 significantly reduced upon *NORM* depletion **[Fig. 3E].** To further understand this, we
261 performed a Gene Ontology (GO) analysis of proteomics data using the DAVID tool. The gene
262 ontology analysis of the proteomics data revealed that biological processes, such as "negative
263 regulation of ubiquitin-protein ligase activity involved in mitotic cell cycle, anaphase-promoting
264 complex-dependent catabolic process, mitotic nuclear envelope disassembly, mitotic spindle
265 assembly, Cell cycle, and G2/M transition of the mitotic cell cycle," were affected **[Fig. 3F].**
266 The Gene Ontology data suggests that *NORM* is involved in regulating mitosis-related
267 pathways. Global transcriptome and proteomics profiling data indicate an overlap between
268 RNA-seq and proteomics profiles. Altogether, our high-throughput data suggests the
269 importance of *NORM* in regulating the cell cycle by associating with mitosis-related pathways.

270 ***NORM* interacts with cell cycle regulatory proteins for chromosome segregation and**
271 **cell cycle regulation**

272 We next sought to investigate the mechanism of action of *NORM* in regulating the cell cycle.
273 We incubated the *in vitro* transcribed full-length biotinylated *NORM* with cell lysate, followed
274 by a pulldown of the *NORM*-protein complex using streptavidin beads **[FIG. 4A]**. *NORM*
275 showed interaction with numerous proteins, including cell cycle regulatory proteins CALM2,
276 CDC5L, SPOUT1, KHDRBS1, Nsun2, and Plk1, out of which polo-like kinase 1 (Plk1)

277 seemed to be interesting, as Plk1 is required for entry of cells into mitosis. Our previous results
278 showed a defect in the G2/M transition under NORM depletion conditions [FIG. 4B & **C]**. The
279 *NORM*-Plk1 interaction was confirmed by performing RNA immunoprecipitation, which
280 showed significant enrichment (~3-fold) of *NORM* in the Plk1 immunoprecipitated **[FIG. 4D]**.
281 Interestingly, we also observed a marginal decline in Plk1 protein levels upon *NORM* depletion
282 **[FIG. 4E]**. Plk1 is one of the major kinases in mitosis, phosphorylating a multitude of substrates
283 at various subcellular locations to regulate mitotic events. Plk1 is essential for the proper
284 assembly of spindles, centrosome maturation, and the attachment of microtubules to
285 kinetochores. We then investigate the role of *NORM* on Plk1's localization at different
286 subcellular locations. We observed differential localization of Plk1 at various subcellular
287 locations, with some defects, in the *NORM*-depleted condition **[FIG. 4F].** To understand the
288 role of *NORM* on Plk1 localization at kinetochores and centrosomes, we examined the level
289 of Plk1 at kinetochores in control versus *NORM* depletion conditions using
290 immunofluorescence. We observed a significantly reduced intensity of Plk1 at kinetochores
291 upon *NORM* depletion compared to control cells, suggesting that *NORM* depletion affected
292 Plk1 localization at kinetochores **[FIG. 4 G&H].** We next sought to determine the effect of
293 *NORM* depletion on chromosome segregation. We observed that depletion of *NORM* leads to
294 defective chromosome segregation, marked by the misalignment of chromosomes during
295 mitosis, and a significantly higher number of cells showed lagging chromosomes at the spindle
296 pole **[Fig. 4 I & J]**.
297
298 ***NORM* depletion hampered the interaction between PLK1 and Bub1**
299 Next, to elucidate the mechanism of reduced localization of Plk1 at kinetochores, we examined
300 the effect of *NORM* depletion on the interaction of key regulatory proteins involved in mitosis.
301 With the help of string analysis, we found that many cell cycle regulatory proteins, such as
302 cyclin B, CENP-E, and Bub1, are known to interact with Plk1 **[FIG. 5A]**. The interaction
303 between Bub1 and Plk1 is crucial for the localization of Plk1 at kinetochores. Plk1 interacts
304 with Bub1 through its polo-box domain (PBD) and phosphorylates Bub1**.** First, we checked if
305 there was any effect of *NORM* depletion on the level of Bub1. We checked the kinetochore
306 localization of Bub1 in control and *NORM*-depleted cells. We observed a marginal change in
307 Bub1 intensity at the kinetochore upon *NORM* depletion **[FIG. 5B & C]**, and no significant
308 change was observed at the protein level of Bub1 upon *NORM* depletion **[FIG. 5D]**. We then
309 checked the effect of *NORM* on the interaction between Plk1 and Bub1. Interestingly, when
310 we immunoprecipitated Plk1, it was able to co-immunoprecipitate Bub1 along with it; however,
311 upon *NORM* depletion, the interaction between Plk1 and Bub1 was hampered, as Plk1 failed
312 to co-immunoprecipitate Bub1 **[FIG. 5E]**. The interaction was validated by performing reverse
313 Co-immunoprecipitation in which an antibody against Bub1 was used to immunoprecipitate

314 Bub1. Reverse Co-IP also showed that upon *NORM* depletion, the interaction between Plk1
315 and Bub1 was hampered **[FIG. 5F]**. It is known that CDK1 phosphorylates Bub1 at the T609
316 residue, and this phosphorylation is essential for the interaction between PLK1 and Bub1 (25)**.**
317 A mitosis-specific anti-MPM2 antibody can be used to detect Bub1 phosphorylated at the T609
318 residue, and phosphorylation of Bub1 at T609 is crucial for the Plk1-Bub1 interaction and the
319 localization of Plk1 at the kinetochore (26)**.** Considering the importance of Bub1 T609 in Plk1
320 interaction, we checked the effect of *NORM* depletion on Bub1 phosphorylation. We
321 immunoprecipitated Bub1 using an anti-Bub1 antibody and assessed the phosphorylation
322 status of Bub1 at T609 using an anti-MPM2 antibody. Interestingly, we observed that *NORM*
323 depletion led to a significant reduction in Bub1 phosphorylation at the T609 residue **[FIG. 5G**
324 **& H]**, indicating that *NORM* is involved in mediating Bub1 phosphorylation. The depletion of
325 *NORM* resulted in a decrease in Bub1 phosphorylation, ultimately hindering Bub1's interaction
326 with Plk1**.** Altogether, these results suggest that the *NORM* is involved in mediating the
327 interaction between Plk1 and Bub1 through the phosphorylation of Bub1 at T609.

328

329 ***NORM* mediates the binding of Nsun2 on CDK1 mRNA to stabilize CDK1 protein**

330 We investigated Bub1's upstream targets to gain a deeper mechanistic understanding of how
331 *NORM* regulates the phosphorylation of Bub1. It is known that Bub1 is phosphorylated at T609
332 by cyclin-dependent kinase 1 (CDK1). Therefore, we explore any potential association
333 between *NORM* and CDK1. Our RNA pulldown data showed that *NORM* lncRNA also interacts
334 with the tRNA methyltransferase Nsun2 (Misu). We validated this interaction by performing an
335 RNA pulldown followed by western blotting to verify the presence of Nsun2 **[Fig. 6A]**. Nsun2
336 binds to CDK1 mRNAs. It stabilizes them at the protein level by methylating them. Next, we
337 examined the effect of *NORM* depletion on Nsun2 at the protein level**.** We found no apparent
338 change in Nsun2 at the protein level, indicating that *NORM* does not directly control Nsun2
339 expression **[Fig. 6B].** Next, we examined the effect of *NORM* depletion on Nsun2 binding to
340 CDK1 mRNA with RNA-immunoprecipitation **[Fig. 6D]**. Interestingly, our RNA-IP with anti-
341 Nsun2 antibody showed that upon depletion of NORM, CDK1 enrichment on Nsun2 was
342 considerably lower than in control cells **[Fig. 6D].** These results suggested that *NORM*
343 depletion inhibits Nsun2's propensity to bind to CDK1 mRNA. Next, we checked the effect of
344 reduced binding on the CDK1 protein level. Immunoblotting data suggested that the CDK1
345 was reduced at the protein level upon NORM depletion [Fig. 6E], suggesting that the reduced
346 level of Nsun2 binding of CDK1 mRNA was hampered by *NORM* depletion, and hence it
347 resulted in reduced stability of CDK1 protein. This reduced level of CDK1 resulted in
348 decreased phosphorylation of Bub1 at T609, ultimately hindering the interaction between Plk1

349 and Bub1. Overall, the evidence suggests the necessity of *NORM* for chromosomal
350 segregation and normal cell cycle progression by mediating Nsun2's binding to CDK1 mRNA
351 and modulating the interaction between Bub1 and Plk1.

352

353 **Discussion:**

354 In this study, we have demonstrated that *NORM*, a long noncoding RNA, plays a crucial role
355 in regulating cell cycle progression from the G2 to M phase. We observed that *NORM* shows
356 an elevated level of expression in the G2 phase. Multiple studies have demonstrated that
357 lncRNAs exhibit tissue- and cell-stage-specific expression. This tissue- and cell-specific
358 expression is often associated with the function of lncRNAs in that cell or tissue. The
359 Kannanganattu V Prasanth group has demonstrated that more than 2,000 long noncoding
360 RNAs (lncRNAs) exhibit periodic expression during the cell cycle. (27). An elevated level of
361 lncRNA is found to be associated with cell stage-specific regulation of the cell cycle phases in
362 a cell stage-specific manner. Therefore, this periodic expression of *NORM* may play a crucial
363 role in regulating the cell cycle. Indeed, we found that when we depleted *NORM* cells, they
364 were arrested at the G2/M phase and were unable to move to the G1 phase upon release.
365 The arrest of cells may be due to the defective assembly of proteins required for mitotic
366 progression. Bida *et al.* also demonstrated that a mitosis-associated long noncoding RNA
367 (lncRNA), MA-linc1, is essential for mitosis. In the absence of lncRNA-MA, cells are unable to
368 progress from mitosis to the G1 phase of the cell cycle.

369 We evaluated the role of *NORM* in regulating cellular proliferation and found that *NORM* plays
370 a crucial part in this process, with depletion of *NORM* resulting in reduced cell proliferation.
371 The G2 phase is a critical phase for cell proliferation, as it determines the cell's fate, whether
372 it will progress into the M phase and divide into two daughter cells. Other evidence also
373 suggests that lncRNA depletion causes cell cycle arrest, leading to a decrease in cellular
374 proliferation.(28)**.** Reduced cellular proliferation was accompanied by an increase in the rate
375 of apoptosis and an increase in the level of DNA damage. When a cell is arrested at any
376 checkpoint for an extended period, the apoptotic cascade is activated**.** We also observed that
377 cells were arrested for a longer time in the G2/M phase. This arrest may have triggered the
378 apoptotic cascade, leading to an increased rate of apoptosis.

379 At the molecular level, a cell's entry into each phase is regulated by various types of cyclins,
380 cyclin-dependent kinases (CDKs), cyclin kinase inhibitors, and specific transcription factors.
381 We observe a significant change in the protein level of CDK1 upon *NORM* depletion. CDK1 is
382 a key regulator of the G2 and M phases of the cell cycle. It, along with cyclin A and Cyclin B,
383 regulates cell entry from the G2 phase to the M phase (29–32). A decrease in the level of

384 CDK1 is one possible reason cells are arrested at the G2/M boundary, and this defect also
385 causes defects in mitotic cells.

386 Through RNA sequencing analysis and proteomics analysis, we found that pathways such as
387 the Regulation of mitotic cell cycle phase transition and the G2/M transition of the mitotic cell
388 cycle were affected. This suggests that *NORM* plays a crucial role in cell cycle progression.
389 DE mRNAs, such as BRCA1, FBXO6, and PCNT, which are involved in cell cycle regulation,
390 were significantly affected. BRCA1 plays a crucial role in regulating the cell cycle(33,34).
391 PCNT is a significant protein that helps in assembling the PCM complex for centrosome
392 maturation(35–37). Therefore, alterations in various genes related to cell cycle progression
393 could have resulted in changes to biological processes associated with the cell cycle.
394 Proteomics analysis also demonstrated that many proteins and the pathways related to cell
395 proliferation and cell cycle were affected.

396 In this study, we observed a significant decrease in Plk1 localization at the kinetochore. At
397 kinetochore Plk1 interacts with Bub1, BubR1 and MAD2 proteins(38–41). The interaction of
398 Plk1 with these proteins is essential for the nucleation of PCM components, including PCNT
399 (36,42). The interaction of Plk1 at the kinetochore facilitates the attachment of the kinetochore
400 to the microtubules (MT). Lera et al. observed a similar result, showing that Plk1 inhibition can
401 cause chromosome missegregation, characterized by lagging chromosomes (43). Therefore,
402 the reduced Plk1 localization at the kinetochore may have impacted the target proteins CENP-
403 U, BubR1, PICH, CLIP-170, CLASP2, Survivin, USP16, and RSF1, for example, including
404 Sgt1 phosphorylation, which could result in improper attachment of microtubules to the
405 kinetochore.(44). PLK1 phosphorylates CENP-Q by binding to CENP-U, and the absence of
406 phosphorylation can lead to chromosome missegregation(45).

407 The interaction between Bub1 and Plk1 is crucial for the proper segregation of chromosomes
408 during cell division. In our study, we observed that *NORM* depletion hampers the interaction
409 between these two proteins. It has been reported in studies that Bub1 becomes
410 phosphorylated at its T609 residue by CDK1, a crucial event for the binding of Bub1 to the
411 PBD domain of Plk1. So, the reduced interaction between Bub1 and Plk1 is a consequence
412 of the reduced CDK1-mediated phosphorylation on Bub1 T609. Plk1 also interacts with CENP-
413 U, along with Bub1, at the kinetochore for chromosome segregation; however, this study has
414 not explored the effect of the interaction between CENP-U and Plk1. In our study, we observed
415 that in the absence of *NORM*, the binding of Nsun2 on CDK1 mRNA was significantly reduced.
416 Other studies have also demonstrated the importance of Nsun2 binding to CDK1 mRNA and
417 its significance in the translation of CDK1 mRNA by mediating methylation. Although our data
418 suggested a direct interaction between the Nsun2 protein and *NORM*, we did not observe a

direct interaction between NORM and CDK1 mRNA, indicating that *NORM* lncRNA and CDK1 mRNA do not form an RNA-RNA interaction complex. This suggests possibilities other than a direct RNA-RNA interaction. One of the limitations of our study is that we have not explored in detail how exactly the *NORM* mediates the interaction between Nsun2 and CDK1 mRNA, nor whether there is any change in the methylation of CDK1 mRNA. However, we speculate that *NORM* acts as a Guide lncRNA for Nsun2 protein to mediate the methylation of CDK1 mRNA, thereby increasing its translation and subsequently phosphorylating Bub1 at T609. Various studies have shown that lncRNAs can exert their functions by acting as a guide molecule for the protein (46).

MATERIALS AND METHODS:

Cell culture:

HeLa cells and Wi-38 cells were cultured in DMEM and MEM, respectively, supplemented with high glucose and 10% fetal bovine serum (FBS), as well as a penicillin-streptomycin antibiotics solution (Gibco). Cells were maintained at 37°C in a humidified atmosphere of 5% CO2.

Antisense oligonucleotide treatment

Transient transfection of cells was performed using. For transfection, LNA GapmeRs Phosphorothioate internucleosidic linkage-modified antisense oligonucleotides were diluted in Opti-MEM. *NORM* Gapmers were used at a final concentration of 100 nM, twice (48 hours apart) within a 24-hour gap, to deplete Human *NORM*.

Flow cytometry:

PI-Flow cytometry was used to analyze the distribution of cell cycle phases. Cells were harvested using a scraper and then collected by centrifugation. Cells were washed with 1X PBS (phosphate-buffered saline) and fixed in ethanol for at least 4 to 5 hours or overnight at 4 °C. Cells were washed two times with 1XPBS and then incubated in 500ul of 1X PBS containing 0.1% Triton X-100, 20mg/ml propidium iodide, and 0.01mg/ml RNase A for 30 min at 37ºC. It was followed by cell cycle analysis using a FACSCalibur (BD Bioscience), and the data were analyzed using CellQuest Pro.

For BrdU-propidium iodide (PI), flow cytometry was performed as described earlier (Tripathi et al., 2013). Briefly, S-phase cells were labeled with BrdU at a final concentration of 50 μM and incubated for 1 hour at 37°C. Cells were further resuspended in chilled 0.9% NaCl and then fixed in an equal volume of ethanol, followed by incubation at −20°C for 1 hour. Furthermore, cells were resuspended and incubated in a 2N HCl + 0.5% Triton X-100 solution

452 for 30 minutes at room temperature, followed by washing in 0.1 M Sodium tetraborate solution.
453 Finally, the cells were resuspended in PBS/0.5% Tween-20 + 1% BSA and incubated with the
454 anti-BrdU antibody for 1 hour at RT. The cells were incubated in PBS + PI/Triton X-100 at
455 37°C for 15 min. Cells were analyzed using a FACScalibur flow cytometer (BD Bioscience),
456 and the data were analyzed with CellQuest Pro.

457 For mitotic cell counting, total cells were collected by trypsinization. It was followed by fixing
458 the cells in chilled 70% ethanol. Cells were permeabilized by using 0.25% Triton X-100. Cells
459 were incubated with H3ser10 antibody (Abcam, ab14955) for two hours at room temperature.
460 It was followed by brief washing and blocking of the cells with 1% BSA. Further, cells were
461 incubated with Alexa Fluor 488 secondary antibody for 30 minutes at room temperature.
462 Moreover, finally, cells were incubated with Propidium iodide (PI) containing RNase for 30
463 minutes. Cells were analyzed using a FACScalibur flow cytometer (BD Bioscience), and the
464 data were analyzed with CellQuest Pro.

465 To detect apoptosis, dual staining with Annexin V and propidium iodide (PI) was performed
466 according to the manufacturer's instructions (Invitrogen, cat. no R37174). Briefly, Wi-38 cells
467 were trypsinized, collected, and washed with ice-cold PBS. Cells were resuspended in 500 µL
468 of 1x binding buffer. A drop of Annexin-V FITC was added, and cells were incubated for 15
469 minutes at 25°C in the dark. 5 µL propidium iodide was added before acquiring the cells. Cells
470 were acquired using a BD FACScanto, and data were analyzed with CellQuest Pro.

471 **Total RNA extraction and quantitative real-time PCR (qRT-PCR):**

472 Total RNA was isolated from cells using Trizol reagent (Invitrogen) according to the
473 manufacturer's instructions, and the concentration was estimated using a UV
474 spectrophotometer. Genomic DNA was digested by DNase I (Sigma) treatment. Total RNA
475 was subjected to first-strand cDNA synthesis using Multiscribe Reverse Transcriptase and
476 Random Hexamers (Invitrogen). Transcript levels were quantified by quantitative real-time
477 PCR (qRT-PCR) using gene-specific primers.

478 **RNA-seq analysis:**

479 Whole-transcriptome analysis of control and *NORM*-depleted samples was performed on the
480 Illumina HiSeq 2500 platform to achieve high transcriptome coverage (50-100 million reads
481 per sample). Briefly, Total RNA was isolated by the RNeasy kit (Qiagen). RNA-seq libraries
482 were constructed using total RNA isolated from untreated and *NORM*-depleted samples with
483 the RNeasy kit (Qiagen). Samples were indexed with adaptors and submitted to paired-end
484 sequencing. RNA-seq reads were aligned with Tophat2.0.11 to the human genome. A
485 comparison of expression levels was calculated by using fragments per kilobase of transcripts

per million fragments mapped (FPKM). Gene ontology analysis was performed by using the Database for Annotation, Visualization, and Integrated Discovery (DAVID) tool (https://david.ncifcrf.gov).

Quantitative proteomics by label-free quantitation mass spectrometry

Human lung fibroblast primary cells (WI38) were seeded in 10 cm cell culture plates for both the scrambled and NORM-depleted conditions. Cells were collected and pelleted in 1X PBS. 1X PBS was removed entirely, and the cell pellet was snap-frozen by liquid nitrogen for 20–30 seconds and stored at -80 °C. Urea lysis buffer was used for cell lysis, and the cells were sonicated to ensure complete lysis. Acetone precipitation was performed by incubating overnight at -20 °C with acetone. Urea rehydration buffer was used for the elution of proteins, followed by the removal of salts. An Amicon ultra-0.5 centrifugal filter unit with a 3 kDa cut-off (UFC500394) was used to remove salt and concentrate the sample. Protein was estimated using Pierce reagent, and bovine serum albumin (BSA) was used for plotting the standard curve. An equal amount of protein (50 µg) was digested using the TFE-In solution digestion protocol. Desalting and concentrating peptides or small proteins were performed using a ZipTip with 0.6 µL C18 resin (ZTC18S096). Mass spectrometry sample preparation was performed by adding 0.1% formic acid to dried protein samples. Samples were acquired by injecting a 2 µL sample into the Thermo Scientific Orbitrap Fusion Tribrid LC-MS/MS system. Raw files were transferred to the Proteome Discoverer software for analysis of the sample.

Cell proliferation assay:

Cell viability was assessed using the 3-(4,5-dimethylthiazol-2-yl)-2,5-diphenyltetrazolium bromide (MTT) assay. Briefly, after transfection with *NORM* ASO or scrambled oligos for 48 hours, HeLa cells were trypsinized, and a suspension of 5000 cells was seeded into a 96-well plate. After 24 hours, 20 µL of MTT (5 mg/mL) was added, and the cells were incubated for an additional 4 hours. Then, 150 µL of isopropanol was added to dissolve the crystals. The proliferation ability of cells was assessed at 0 hours, 24 hours, 48 hours, 72 hours, and 96 hours by incubating the cells at 37°C. Absorbance at 570 nm was determined spectrophotometrically by using a microplate reader. Colony-forming ability was checked by the colony formation assay. Briefly, 1,000 cells were seeded in a six-well plate and maintained for 2 weeks, during which the media were replaced every 3 days. Colonies were fixed by PFA and stained by using crystal violet in PBS for 30 minutes. The colony formation ability was assessed by counting stained colonies.

520 **Immunoblotting**

521 Cells were washed twice with PBS and then collected by scraping. A lysis buffer containing
522 protease and phosphatase inhibitor was used for extraction. Loading dye was added directly
523 to the samples, and the samples were denatured by boiling for 5 min at 95°C. The total cell
524 lysate was subjected to SDS-polyacrylamide gel electrophoresis (SDS-PAGE), and proteins
525 were transferred to the PVDF membrane. The membrane was incubated with primary
526 antibodies overnight at 4°C. An appropriate secondary antibody was incubated for 1 hour at
527 room temperature. The antibodies used for immunoblotting were anti-CDK1(Cdc2) (1:1000;
528 Santa Cruz SC-54), anti-PARP (1:1000; Cell signaling technology, 9542), anti-Bax (1:500;
529 Santa Cruz sc493), anti-Bcl2 (1:500; Santa Cruz sc492), anti-Plk1 (1:1000 Abcam ab17056),
530 anti-Cyclin A (1:1000; Santa Cruz sc271682), anti-Cyclin B(1:1000; Santa Cruz sc7393), anti-
531 Cyclin E (1:1000; Santa Cruz sc377100), anti-CDK4(1:1000; Santa Cruz sc23896), anti-
532 Bub1(1:100 ab54893), H3ser10 antibody (1:1000; ab14955;), anti-α-Tubulin (1:5000; Sigma
533 T6199), Anti-mouse IgG, HRP-linked (1:5000; cell signalling technology; 7076), Anti-rabbit
534 IgG, HRP-linked (1:5000; cell signalling technology; 7074).

535 **Immunostaining:**

536 Immunofluorescence was performed as described earlier (Tripathi et al., 2013). Briefly, Wi-38
537 cells, grown on coverslips, were then fixed in 2% PFA for 20 minutes at room temperature
538 (RT) and permeabilized with 0.1% Triton X-100 for 10 minutes on ice. Cells were blocked by
539 incubating with 5% fetal bovine serum (FBS) at room temperature (RT) for 1 hour, followed by
540 incubation with the primary antibody for 2 hours at RT. Incubation with fluorescence-tagged
541 secondary antibody was performed for 1 hour at room temperature. Finally, cells were stained
542 with Hoechst and mounted in mounting media. The antibodies were used are Ki-67 (1:500;
543 Abcam; ab16667), anti-Plk1 (1:100 Abcam; ab17056), anti-α-Tubulin (1:1000; Sigma T6199),
544 anti-Bub1(1:100; Abcam; ab195268), anti-Pericentrin (1:200; Novus; NB 100-61071) CREST
545 (1:500; antibodiesinc; 115-234), Alexa flour 488 donkey anti-rabbit IgG (H+L) (1:1000;
546 Invitrogen; A21206), Alexa flour 594 donkey anti-mouse IgG (H+L) (1:1000; Invitrogen;
547 A21203) images were acquired on Zeiss microscope.

548 **RNA pulldown and Mass spectrometry analysis:**

549 *NORM* was cloned into a pGEMT vector. The plasmid was linearized by using the NcoI
550 restriction enzyme. Purified plasmids were then used for in vitro transcription with a Biotin RNA
551 labeling Mix (Roche). Biotin labeling was done by using T7 polymerase at 37°C for 6 hours.
552 In vitro transcribed RNA was then purified by passing it through a MicroSpin column (Illustra
553 MicroSpin G-25 columns, 27-5325-01, Merck). Fresh lysate was prepared by using Protein
554 extraction buffer (20 mM Tris HCl, pH 7.5, 100 mM KCl,5 mM MgCl2,0.5% NP40) with

555 protease, phosphatase cocktail inhibitors, and RNase inhibitors. The lysate was precleared
556 using magnetic streptavidin Dynabeads (M-280 streptavidin, Cat. No. 11205D, Invitrogen).
557 Biotin-labeled RNA and lysate were incubated on a rotator for 2 hours. It was followed by the
558 addition of magnetic streptavidin Dynabeads to a mixture of RNA-lysate. It was further
559 incubated for 2 hours. Next, protein samples were separated by SDS-PAGE, and bands were
560 visualized by silver staining. For mass spectrometry analysis, the immunoprecipitated protein
561 was washed with 100 mM ammonium bicarbonate. Proteins were prepared for mass
562 spectrometry by digesting with RapiGest at 60°C for 30 minutes and then analysed by mass
563 spectrometry.

564 **RNA Immunoprecipitation:**

565 Cells were washed twice with ice-cold phosphate-buffered saline (PBS). Cells were irradiated
566 with 300mJ/cm^2 in a UV crosslinker. The cell lysate was prepared by using RSB100 lysis buffer
567 (100 mM Tris-Cl, pH 7.4, 100 mM NaCl, 2.5 mM $MgCl_2$, 0.5% NP40, 0.5% Triton X-100) by
568 incubating on ice for 15 minutes. The lysate was centrifuged, and the supernatant was
569 collected. 0.1M DTT, RNase Inhibitor, and DNase I were added to the supernatant. The lysate
570 was precleared by incubating Protein G agarose beads (Pierce, Cat. No. 20398) at 4°C for 1
571 hour, rotating on a rotor shaker. Immunoprecipitation was performed by incubating an equal
572 amount of lysate with an anti-Plk1 antibody (1:100; Abcam, ab17056), an anti-Nsun2 (1:100;
573 Abcam, ab259941), and a mouse IgG antibody (Negative control) overnight on a rotator
574 shaker at 4 °C. Next, protein G agarose beads were added and incubated further for 2 hours.
575 Co-immunoprecipitated RNA was isolated by resuspending the beads in 1 mL of Trizol
576 (Invitrogen). RNA was isolated according to the manufacturer's instructions. cDNA was
577 prepared using 5X PrimeScript RT Master Mix (Takara, cat. no RR036A-1).

578

579 **References:**

580 1. Pavletich NP. Mechanisms of cyclin-dependent kinase regulation: Structures of Cdks,
581 their cyclin activators, and Cip and INK4 inhibitors. J Mol Biol. 1999;287(5):821–8.

582 2. Giacinti C, Giordano A. RB and cell cycle progression. Oncogene. 2006;25:5220–7.

583 3. Holland AJ, Cleveland DW. Losing balance: the origin and impact of aneuploidy in
584 cancer. EMBO Rep [Internet]. 2012;13(6):501–14. Available from:
585 http://dx.doi.org/10.1038/embor.2012.55

586 4. Cleveland DW, Mao Y, Sullivan KF. Centromeres and kinetochores: From epigenetics
587 to mitotic checkpoint signaling. Cell. 2003;112(4):407–21.

588 5. Lara-gonzalez P, Pines J, Desai A. Spindle assembly checkpoint activation and
589 silencing at kinetochores. Semin Cell Dev Biol [Internet]. 2021;117:86–98. Available
590 from: https://doi.org/10.1016/j.semcdb.2021.06.009

591 6. Lara-gonzalez P, Westhorpe FG. The Spindle Assembly Checkpoint. Curr Biol
592 [Internet]. 2012;22(22):R966–80. Available from:
593 http://dx.doi.org/10.1016/j.cub.2012.10.006

594 7. Overlack K, Primorac I, Vleugel M, Krenn V, Maffini S, Hoffmann I, et al. A molecular
595 basis for the differential roles of Bubl and BubR1 in the spindle assembly checkpoint.
596 Elife. 2015;2015(4):1–24.

597 8. Yamagishi Y, Yang CH, Tanno Y, Watanabe Y. MPS1/Mph1 phosphorylates the
598 kinetochore protein KNL1/Spc7 to recruit SAC components. Nat Cell Biol.
599 2012;14(7):746–52.

600 9. Singh P, Pesenti ME, Maffini S, Srinivasamani A, Singh P, Pesenti ME, et al. BUB1
601 and CENP-U , Primed by CDK1 , Are the Main PLK1 Kinetochore Receptors in
602 Mitosis ll BUB1 and CENP-U Primed by CDK1 , Are the Main PLK1 Kinetochore
603 Receptors in Mitosis. Mol Cell [Internet]. 2021;81(1):67-87.e9. Available from:
604 https://doi.org/10.1016/j.molcel.2020.10.040

605 10. Josue E, Nebreda AR, Fernandez M. A Two-Step Inactivation Mechanism of Myt1
606 Ensures CDK1 / Cyclin B Activation and Meiosis I Entry. Curr Biol. 2010;717–23.

607 11. Malumbres M. Cyclin-dependent kinases. Malumbres Genome Biol. 2014;1–10.

608 12. Xing J, Yi J, Cai X, Tang H, Liu Z, Zhang X, et al. NSun2 Promotes Cell Growth via
609 Elevating Cyclin-Dependent Kinase 1 Translation. Mol Cell Biol. 2015;35(23):4043–
610 52.

611 13. Tripathi V, Shen Z, Chakraborty A, Giri S, Freier SM, Wu X, et al. Long Noncoding
612 RNA MALAT1 Controls Cell Cycle Progression by Regulating the Expression of
613 Oncogenic Transcription Factor B-MYB. PLoS Genet. 2013;9(3).

614 14. Wang C, Yang Y, Zhang G, Li J, Wu X, Ma X, et al. Long noncoding RNA EMS
615 connects c-Myc to cell cycle control and tumorigenesis. PNAS. 2019;

616 15. Su C, Wang W, Mo J, Liu F, Zhang H, Liu Y, et al. Long noncoding RNA HOXC - AS3
617 interacts with CDK2 to promote proliferation in hepatocellular carcinoma. Biomark Res
618 [Internet]. 2022;1–15. Available from: https://doi.org/10.1186/s40364-022-00411-2

619 16. Chen W, Zhou Z, Ren Y, Zhang L, Sun L, Man Y, et al. Effects of long non-coding

620 RNA LINC00667 on renal tubular epithelial cell proliferation , apoptosis and renal fi
621 brosis via the miR-19b-3p / LINC00667 / CTGF signaling pathway in chronic renal
622 failure. Cell Signal [Internet]. 2019;54(October 2018):102–14. Available from:
623 https://doi.org/10.1016/j.cellsig.2018.10.016

624 17. Yang H, Yang W, Dai W, Ma Y, Zhang G. LINC00667 promotes the proliferation ,
625 migration , and pathological angiogenesis in non – small cell lung cancer through
626 stabilizing VEGFA by EIF4A3. cell Biol Int [Internet]. 2020;(April):1671–80. Available
627 from: https://doi.org/10.1002/cbin.11361

628 18. Pei Liu, Shuofan Chen, Yangyue Huang, Shuai Xu, Hongcheng Song WZ and NS.
629 LINC00667 promotes Wilms tumor metastasis and stemness by sponging miR-200b
630 c.pdf. cell Biol Int. 2020;

631 19. Ren S, Zhang Y, Yang X, Li X, Zheng Y, Liu Y. N6-methyladenine- induced
632 LINC00667 promoted breast cancer progression through m6A / KIAA1429 positive
633 feedback loop. Bioengineered [Internet]. 2022;13(5):13462–73. Available from:
634 https://doi.org/10.1080/21655979.2022.2077893

635 20. Zhao J, Chen P, Tan C, Cheng X, Zhang W, Shen C. LncRNA LINC00667 gets
636 involved in clear cell renal cell carcinoma development and chemoresistance by
637 regulating the miR-143- 3p / ZEB1 axis. Aging (Albany NY). 2023;15(19):10055–71.

638 21. Li J, Kang J, Liu W, Liu J, Pan G, Mao A, et al. Docetaxel-resistant triple-negative
639 breast cancer cell-derived exosomal lncRNA LINC00667 reduces the
640 chemosensitivity of breast cancer cells to docetaxel via targeting miR-200b-3p/Bcl-2
641 axis. Eur J Histochem. 2022;66.

642 22. Liao B, Yi Y, Zeng L, Wang Z, Zhu X, Liu J, et al. LINC00667 Sponges miR-4319 to
643 Promote the Development of Nasopharyngeal Carcinoma by Increasing FOXQ1
644 Expression. Front Oncol. 2021;10(January):1–10.

645 23. Pan J, Zang Y. LINC00667 Promotes Progression of Esophageal Cancer Cells by
646 Regulating miR - 200b - 3p / SLC2A3 Axis. Dig Dis Sci [Internet]. 2022;67(7):2936–
647 47. Available from: https://doi.org/10.1007/s10620-021-07145-5

648 24. Li J, Guan C, Hu Z, Liu L, Su Z, Kang P, et al. Yin Yang 1 - induced LINC00667 up -
649 regulates pyruvate dehydrogenase kinase 1 to promote proliferation , migration and
650 invasion of cholangiocarcinoma cells by sponging miR - 200c - 3p. Hum Cell
651 [Internet]. 2021;34(1):187–200. Available from: https://doi.org/10.1007/s13577-020-
652 00448-1

653 25. Singh P, Pesenti ME, Maffini S, Carmignani S, Hedtfeld M, Petrovic A, et al. BUB1
654 and CENP-U, Primed by CDK1, Are the Main PLK1 Kinetochore Receptors in Mitosis.
655 Mol Cell [Internet]. 2021;81(1):67-87.e9. Available from:
656 https://doi.org/10.1016/j.molcel.2020.10.040

657 26. Qi W, Tang Z, Yu H. Phosphorylation- and Polo-Box – dependent Binding of Plk1 to
658 Bub1 Is Required for the Kinetochore Localization of Plk1. Mol Biol Cell.
659 2006;17(August):3705–16.

660 27. Hao Q, Zong X, Sun Q, Lin Y, Song YJ, Hashemikhabir S, et al. The S-phase-induced
661 lncRNA SUNO1 promotes cell proliferation by controlling YAP1 / Hippo signaling
662 pathway. Elife. 2020;1–33.

663 28. Zhang X, Wu N, Wang J, Li Z. LncRNA MEG3 inhibits cell proliferation and induces
664 apoptosis in laryngeal cancer via miR-23a/APAF-1 axis. J Cell Mol Med.
665 2019;23(10):6708–19.

666 29. Ubersax JA, Woodbury EL, Quang PN. Targets of the cyclin-dependent kinase Cdk1.
667 Nature. 2003;859–64.

668 30. Porter LA, Donoghue DJ. Cyclin B1 and CDK1 : Nuclear localization and upstream
669 regulators Cyclin B1 and CDK1 : nuclear localization and upstream regulators. Prog
670 Cell Cycle Res. 2003;(February).

671 31. Gavet O, Pines J. Progressive Activation of CyclinB1-Cdk1 Coordinates Entry to
672 Mitosis. Dev Cell [Internet]. 2010;18(4):533–43. Available from:
673 http://dx.doi.org/10.1016/j.devcel.2010.02.013

674 32. Cerqueira A, Hunt S, Tardy C, Newton K, Santamarı D, Dubus P, et al. Cdk1 is
675 sufficient to drive the mammalian cell cycle. Nature. 2007;448(August):811–6.

676 33. Deng CX. BRCA1: Cell cycle checkpoint, genetic instability, DNA damage response
677 and cancer evolution. Nucleic Acids Res. 2006;34(5):1416–26.

678 34. Xu B, Kim S, Kastan MB. Involvement of Brca1 in S-Phase and G2-Phase
679 Checkpoints after Ionizing Irradiation. Mol Cell Biol. 2001;21(10):3445–50.

680 35. Kim J, Kim J, Rhee K. PCNT is critical for the association and conversion of centrioles
681 to centrosomes during mitosis. J Cell Sci. 2019;132(6).

682 36. Kim J, Lee K, Rhee K. PLK1 regulation of PCNT cleavage ensures fidelity of centriole
683 separation during mitotic exit. Nat Commun. 2015;

684 37. Tibelius A, Marhold J, Zentgraf H, Heilig CE, Neitzel H, Ducommun B, et al.

685 Microcephalin and pericentrin regulate mitotic entry via centrosome-associated Chk1.
686 J Cell Biol. 2009;185(7):1149–57.

687 38. Schmucker S, Sumara I. Molecular dynamics of PLK1 during mitosis. Mol Cell Oncol.
688 2014;(June):1–9.

689 39. Lee K, Rhee K. PLK1 phosphorylation of pericentrin initiates centrosome maturation
690 at the onset of mitosis. J Cell Biol. 2011;195(7):1093–101.

691 40. Gheghiani L, Loew D, Gavet O. PLK1 Activation in Late G2 Sets Up Commitment to
692 Mitosis. Cell Rep. 2017;2060–73.

693 41. Ikeda M, Tanaka K. Plk1 bound to Bub1 contributes to spindle assembly checkpoint
694 activity during mitosis. Sci Rep [Internet]. 2017;(September 2016):1–15. Available
695 from: http://dx.doi.org/10.1038/s41598-017-09114-3

696 42. Lee K, Rhee K. PLK1 phosphorylation of pericentrin initiates centrosome maturation
697 at the onset of mitosis. J Cell Sci. 2011;195(7):1093–101.

698 43. Lera RF, Norman RX, Dumont M, Dennee A, Martin-koob J, Fachinetti D, et al. Plk 1
699 protects kinetochore – centromere architecture against microtubule pulling forces.
700 EMBO Rep. 2019;1–16.

701 44. Liu XS, Song B, Tang J, Liu W, Kuang S, Liu X. Plk1 Phosphorylates Sgt1 at the
702 Kinetochores To Promote Timely. 2012;32(19):4053–67.

703 45. Kang YH, Park C, Kim T, Soung N, Bang JK, Kim BY, et al. Mammalian Polo-like
704 Kinase 1-dependent Regulation of the PBIP1-CENP-Q Complex at Kinetochores * □.
705 J Biol Chem [Internet]. 2011;286(22):19744–57. Available from:
706 http://dx.doi.org/10.1074/jbc.M111.224105

707 46. Zhao Z, Sentürk N, Song C, Grummt I. lncRNA PAPAS tethered to the rDNA
708 enhancer recruits hypophosphorylated CHD4 / NuRD to repress rRNA synthesis at
709 elevated temperatures. GENES Dev. 2018;836–48.

710

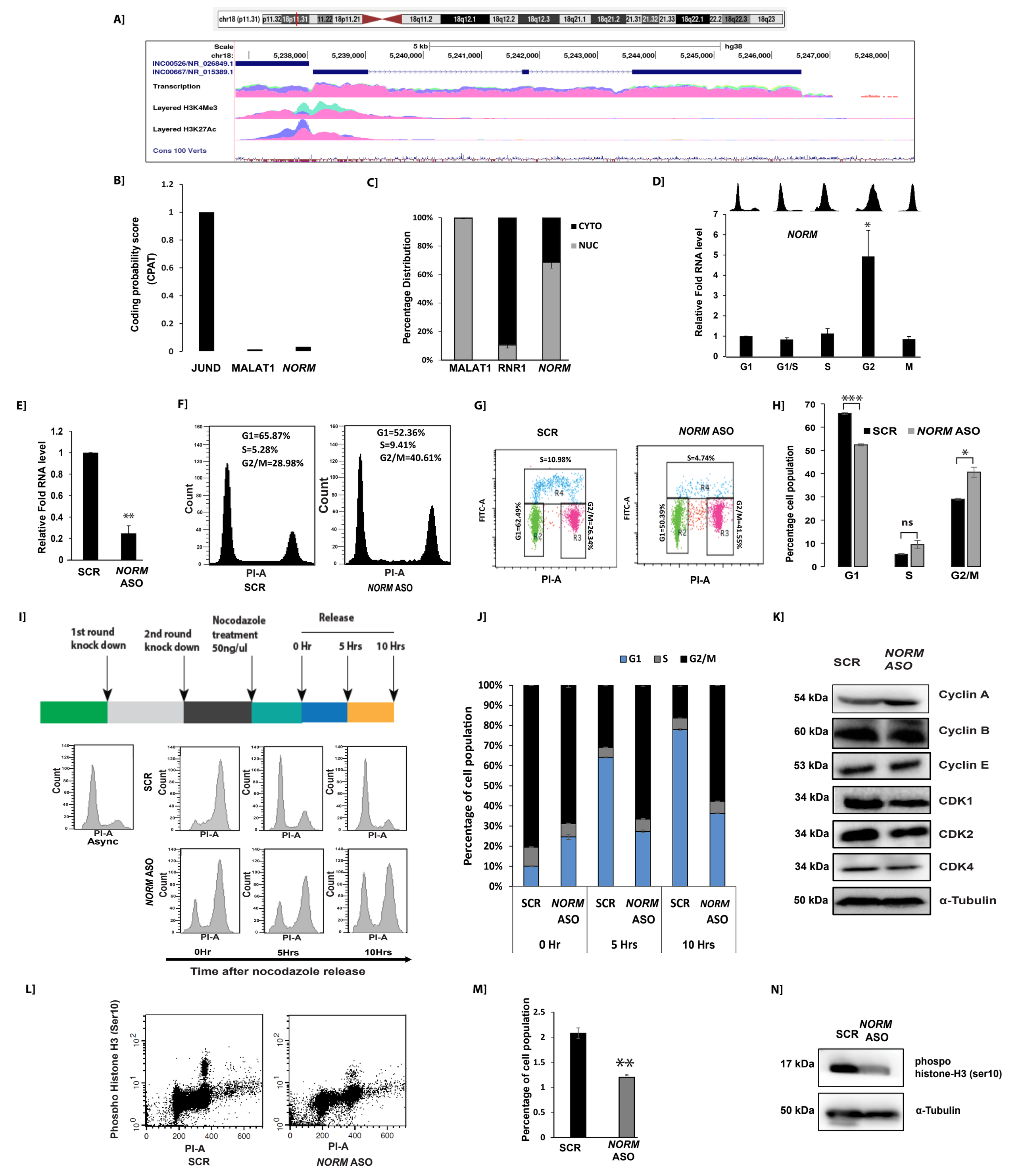
A]
chr18 (p11.31)
Scale
chr18:
5 kb
hg38
INC00526/NR_026849.1
INC00667/NR_015389.1
Transcription
Layered H3K4Me3
Layered H3K27Ac
Cons 100 Verts
B]
Coding probability score (CPAT)
JUND
MALAT1
NORM
C]
Percentage Distribution
CYTO
NUC
MALAT1
RNR1
NORM
D]
Relative Fold RNA level
NORM
G1
G1/S
S
G2
M
E]
Relative Fold RNA level
SCR
NORM ASO
F]
G1=65.87%
S=5.28%
G2/M=28.98%
G1=52.36%
S=9.41%
G2/M=40.61%
Count
PI-A
SCR
NORM ASO
G]
SCR
NORM ASO
S=10.98%
S=4.74%
G1=62.49%
G2/M=26.34%
G1=50.39%
G2/M=41.55%
FITC-A
PI-A
H]
Percentage cell population
SCR
NORM ASO
ns
G1
S
G2/M
I]
1st round knock down
2nd round knock down
Nocodazole treatment 50ng/ul
Release
0 Hr
5 Hrs
10 Hrs
Count
PI-A
Async
SCR
NORM ASO
0Hr
5Hrs
10Hrs
Time after nocodazole release
J]
G1
S
G2/M
Percentage of cell population
SCR
NORM ASO
0 Hr
5 Hrs
10 Hrs
K]
SCR
NORM ASO
54 kDa
Cyclin A
60 kDa
Cyclin B
53 kDa
Cyclin E
34 kDa
CDK1
34 kDa
CDK2
34 kDa
CDK4
50 kDa
α-Tubulin
L]
Phospho Histone H3 (Ser10)
PI-A
SCR
NORM ASO
M]
Percentage of cell population
SCR
NORM ASO
N]
SCR
NORM ASO
17 kDa
phospo histone-H3 (ser10)
50 kDa
α-Tubulin

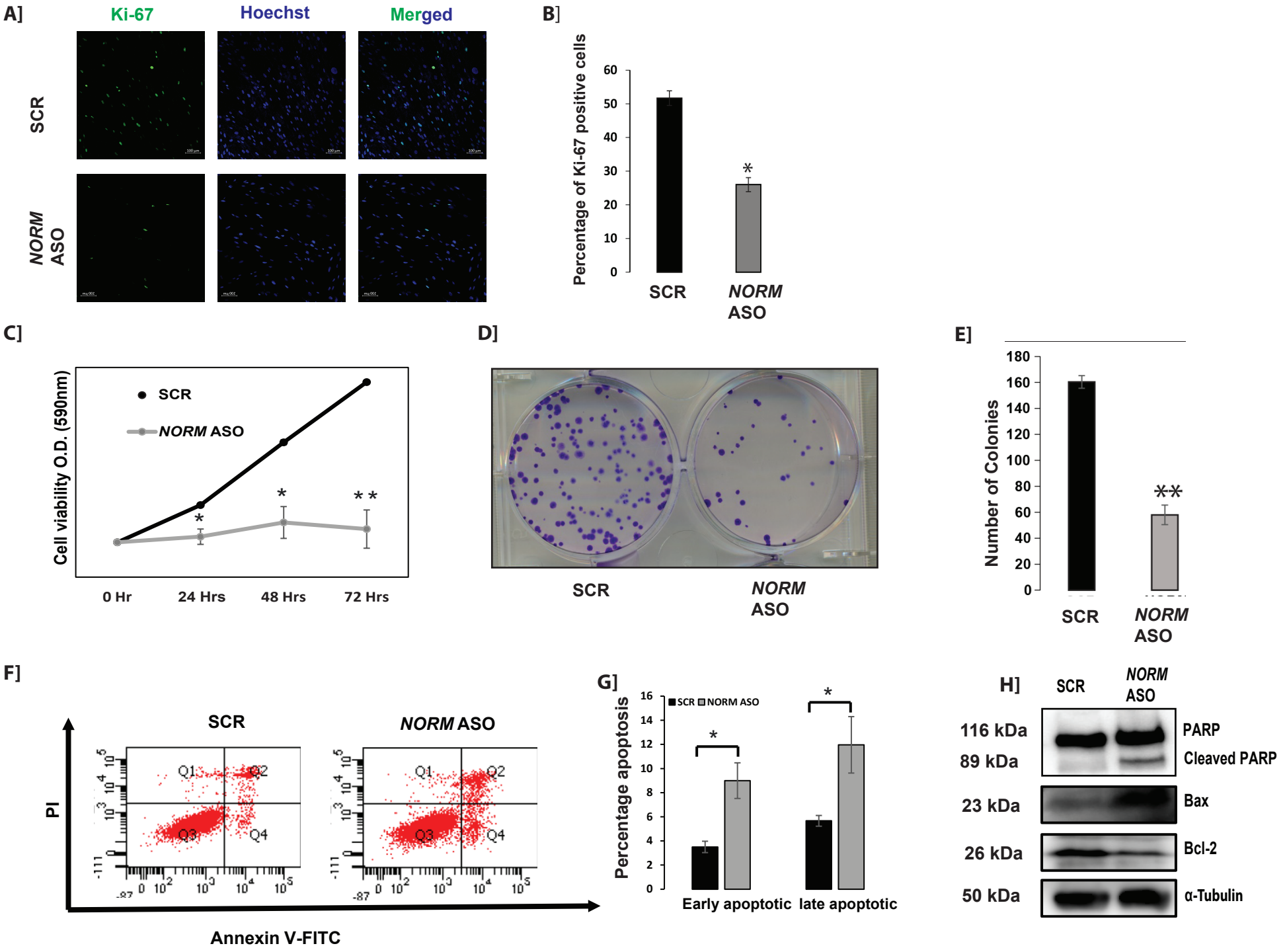
A]
Ki-67
Hoechst
Merged
SCR
NORM ASO
B]
Percentage of Ki-67 positive cells
60
50
40
30
20
10
0
*
SCR
NORM ASO
C]
Cell viability O.D. (590nm)
SCR
NORM ASO
*
*
* *
0 Hr
24 Hrs
48 Hrs
72 Hrs
D]
SCR
NORM ASO
E]
Number of Colonies
180
160
140
120
100
80
60
40
20
0
**
SCR
NORM ASO
F]
SCR
NORM ASO
PI
Q1
Q2
Q3
Q4
Annexin V-FITC
G]
Percentage apoptosis
SCR NORM ASO
*
*
Early apoptotic
late apoptotic
H]
SCR
NORM ASO
116 kDa
89 kDa
PARP
Cleaved PARP
23 kDa
Bax
26 kDa
Bcl-2
50 kDa
α-Tubulin

A]

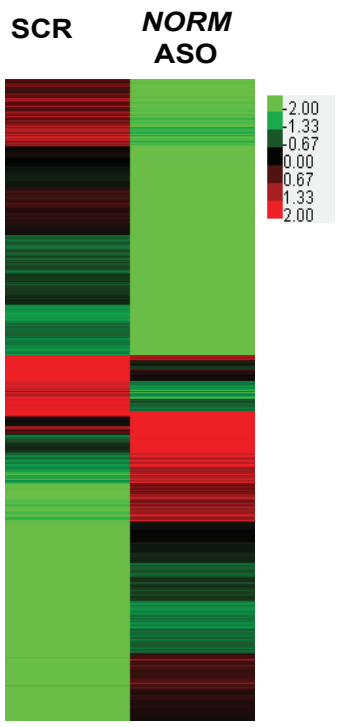

B]

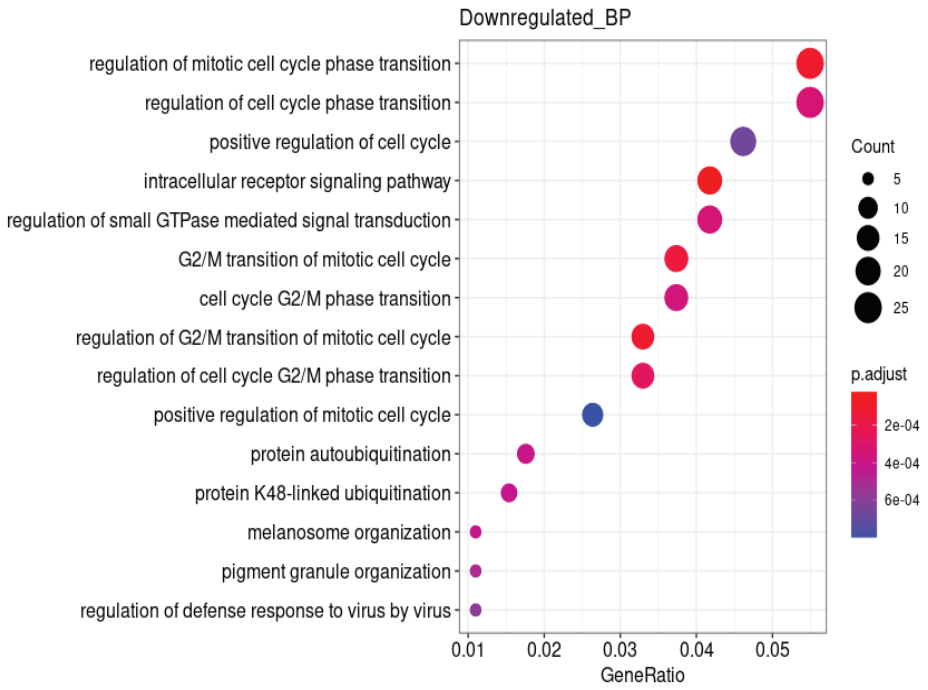

C]

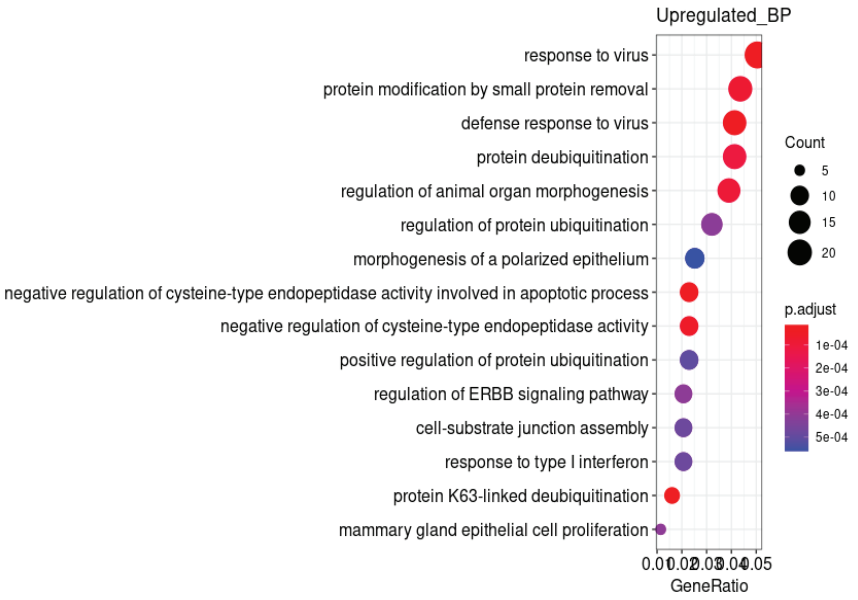

D]

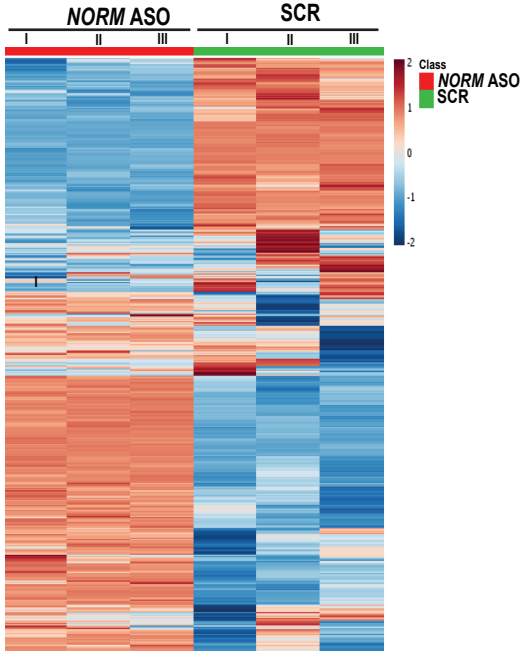

E]

Upregulated

Gene	Fold change
TGM2	18.648
PSMD1	18.52
CLTC	15.713
PSMD2	14.44
PSMA4	12.72
ANXA4	12.352
BUB3	11.486
BANF1	11.348
RCC1	10.743
DDB1	9.771
PRKDC	9.565
DYNC1H1	9.426
CTTN	9.028
NUP50	6.697
SBDS	6.387
PSMB1	6.372
GNAI2	6.25
HMGA2	6.021

Downregulated

Protein	Fold change
PDGFRB	0.016
PTMS	0.025
COL1A1	0.096
CD2AP	0.131
LAMB2	0.133
YWHAB	0.191
COL1A2	0.242
CDK1	0.263
RAD21	0.285
PPP2R5D	0.296
MCM3	0.382
RBX1	0.397
YWHAG	0.422
SMC4	0.435
CCDC124	0.436
YWHAE	0.438
MCM5	0.48

F]

Downregulated

Pathway	Count
negative regulation of apoptotic process	26
cell proliferation	22
negative regulation of ubiquitin-protein ligase activity involved in mitotic cell cycle	17
positive regulation of ubiquitin-protein ligase activity involved in regulation of mitotic cell cycle transition	17
anaphase-promoting complex-dependent catabolic process	17
DNA damage response, detection of DNA damage	7
mitotic nuclear envelope disassembly	6
mitotic spindle organization	5
mitotic spindle assembly	5

Upregulated

Pathway	Count
PI3K-Akt signaling pathway	9
cell division	8
Cell cycle	8
cell migration	5
G2/M transition of mitotic cell cycle	4
regulation of actin cytoskeleton organization	3
positive regulation of protein insertion into mitochondrial membrane involved in apoptotic signaling pathway	3
positive regulation of DNA biosynthetic process	2

A]

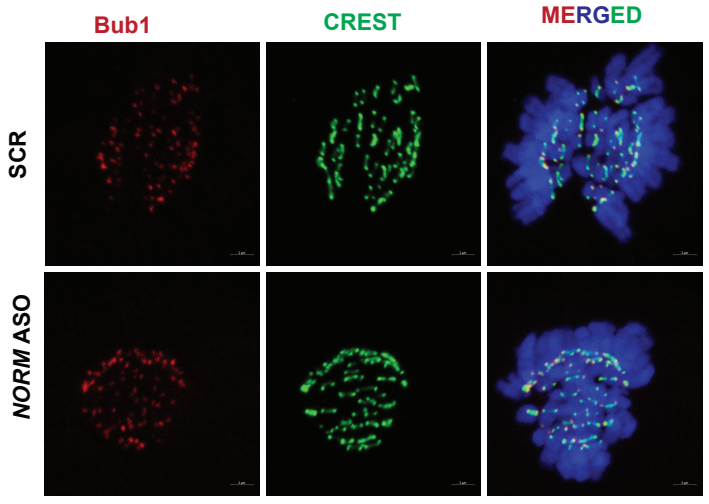
Bub1
CREST
MERGED
SCR
NORM ASO

C]

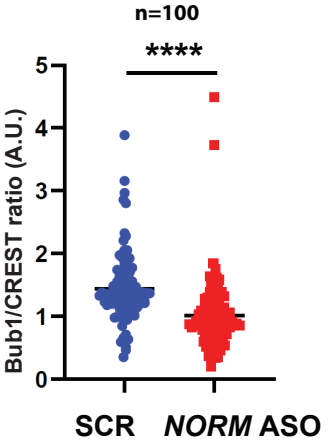
n=100
****
Bub1/CREST ratio (A.U.)
0
1
2
3
4
5
SCR
NORM ASO

D]

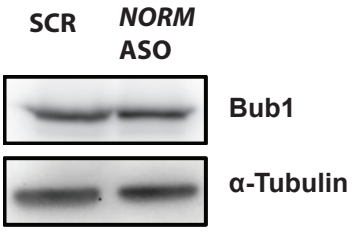
SCR
NORM ASO
Bub1
α-Tubulin

B]

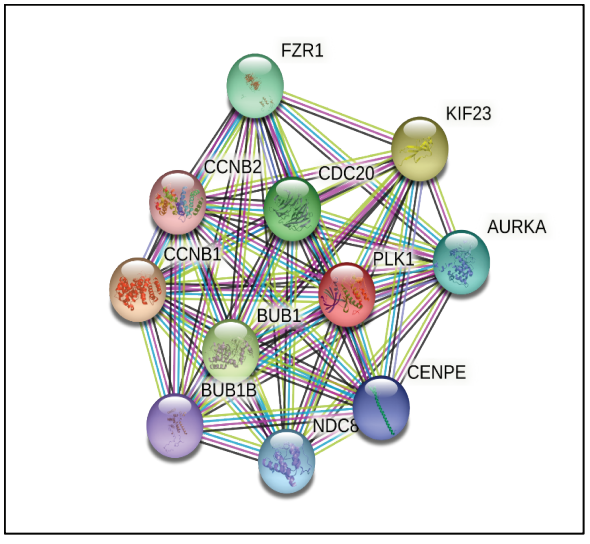
FZR1
KIF23
CCNB2
CDC20
AURKA
CCNB1
PLK1
BUB1
CENPE
BUB1B
NDC8

E]

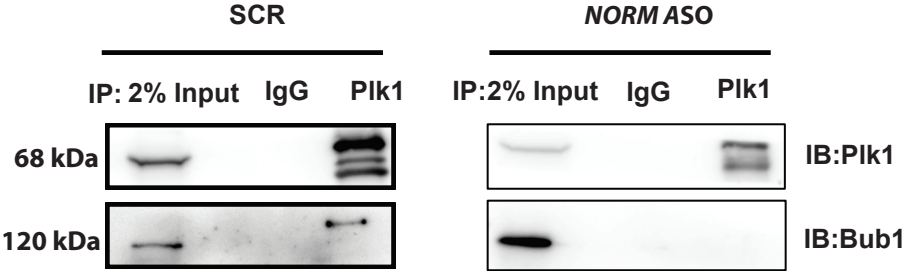
SCR
NORM ASO
IP: 2% Input
IgG
Plk1
IP:2% Input
IgG
Plk1
68 kDa
120 kDa
IB:Plk1
IB:Bub1

F]

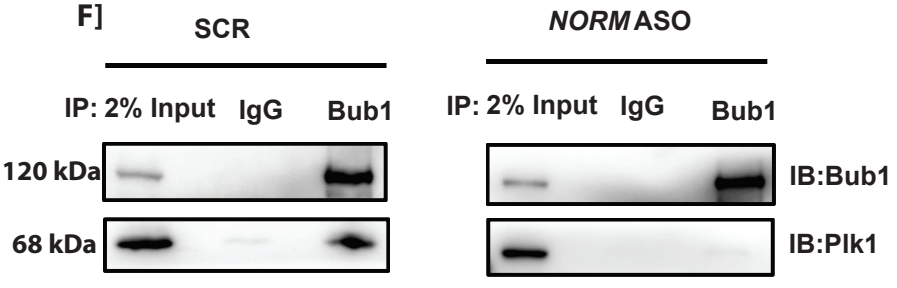
SCR
NORM ASO
IP: 2% Input
IgG
Bub1
IP: 2% Input
IgG
Bub1
120 kDa
68 kDa
IB:Bub1
IB:Plk1

G]

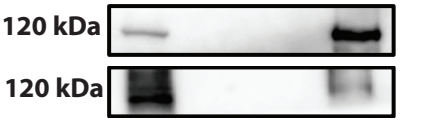
SCR
IP:
2% Input
IgG
Bub1
120 kDa
120 kDa

H]

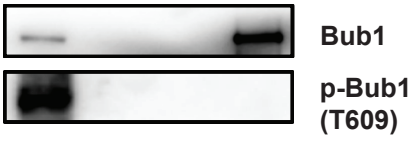
NORM ASO
IP:2% Input
IgG
Bub1
Bub1
p-Bub1 (T609)

A]

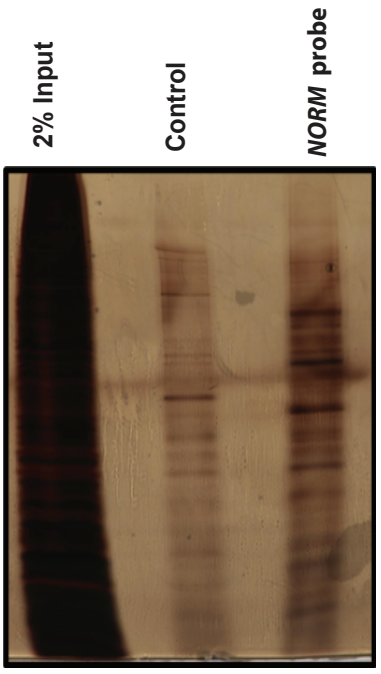

B]

Gene	Sum PEP score
XRN2	5.424
FUS	3.806
GNL3	9.488
KHDRBS1	5.627
NSUN2	3.706
ARHGEF2	1.483
SPOUT1	1.524
XRCC6	5.008
CALM2	7.023
CDC5L	3.339
GAPDH	2.324
MRPS26	3.483
PLK1	1.833
RPS27A	2.352
RPS6	8.711
TUBA1B	18.025
TUBB	20.338

C]

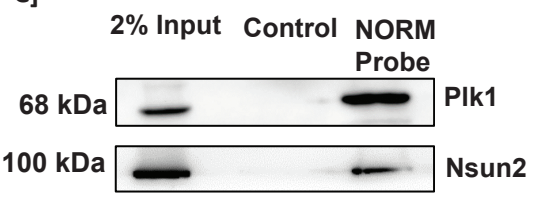

D]

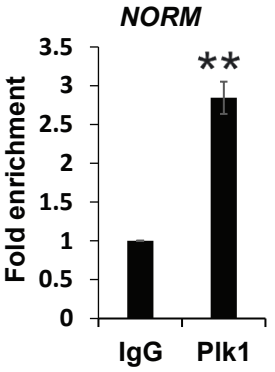

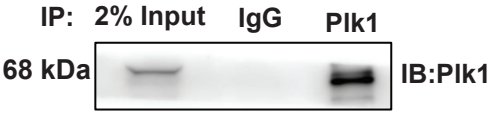

E]

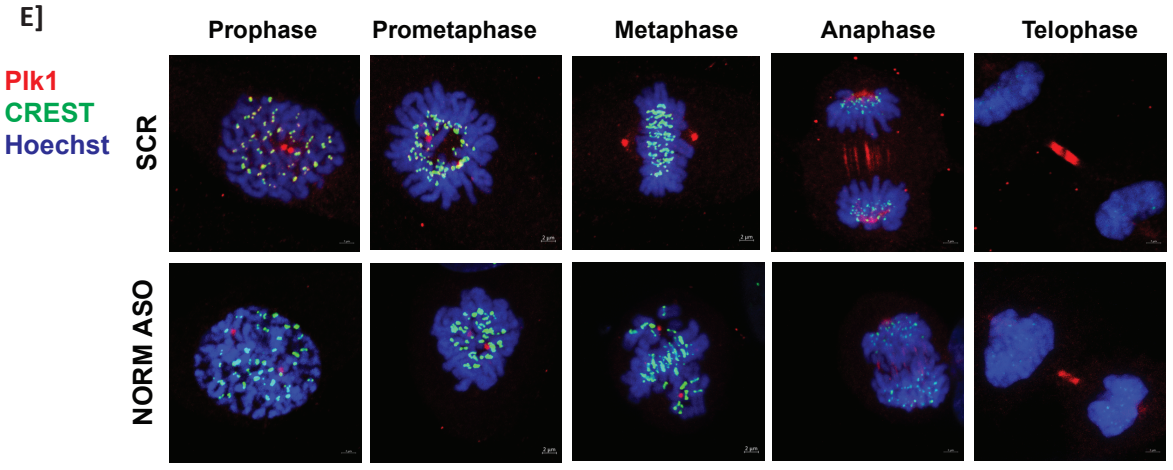

F]

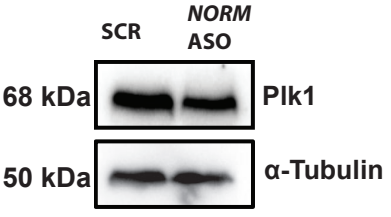

G]

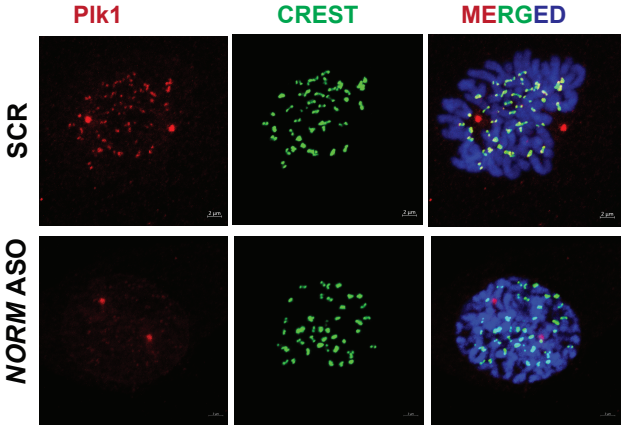

H]

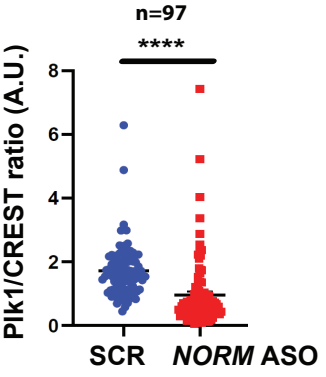

I]

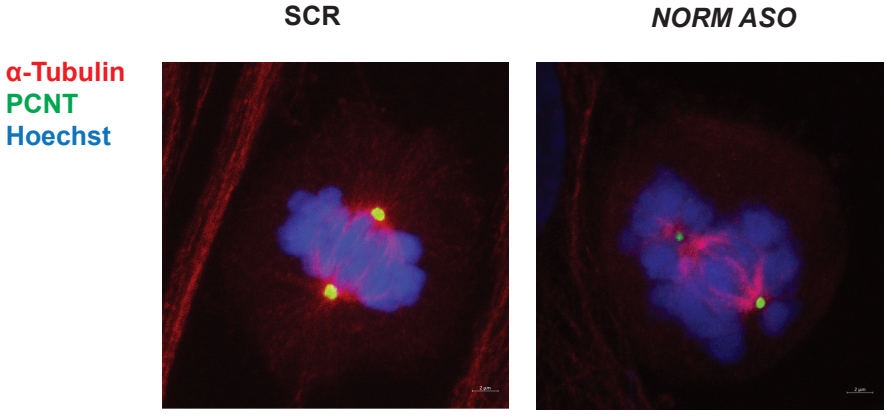

J]

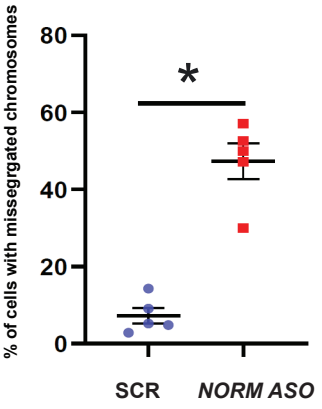

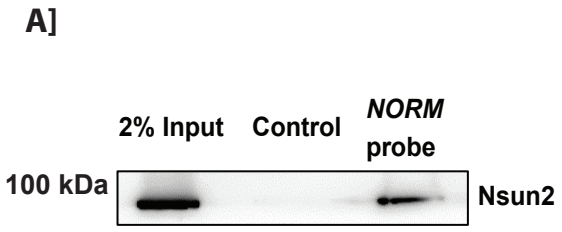
A]
2% Input
Control
NORM probe
100 kDa
Nsun2

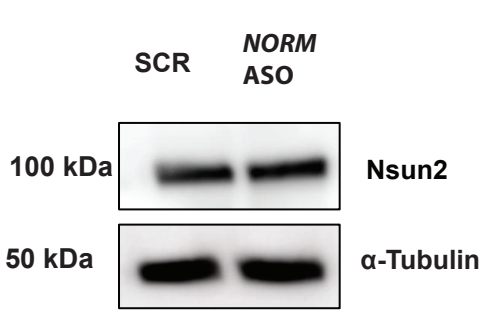
B]
SCR
NORM ASO
100 kDa
Nsun2
50 kDa
α-Tubulin

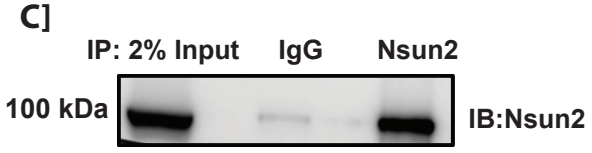
C]
IP: 2% Input
IgG
Nsun2
100 kDa
IB:Nsun2

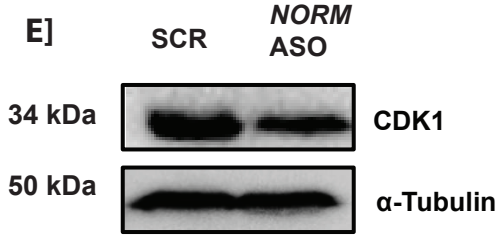
E]
SCR
NORM ASO
34 kDa
CDK1
50 kDa
α-Tubulin

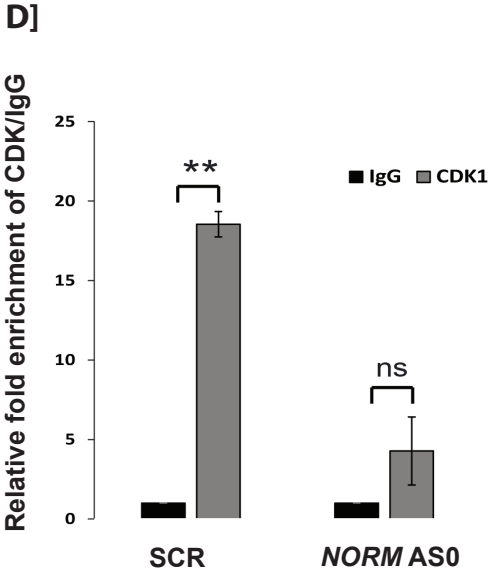
D]
Relative fold enrichment of CDK/IgG
25
20
15
10
5
0
**
ns
IgG
CDK1
SCR
NORM AS0

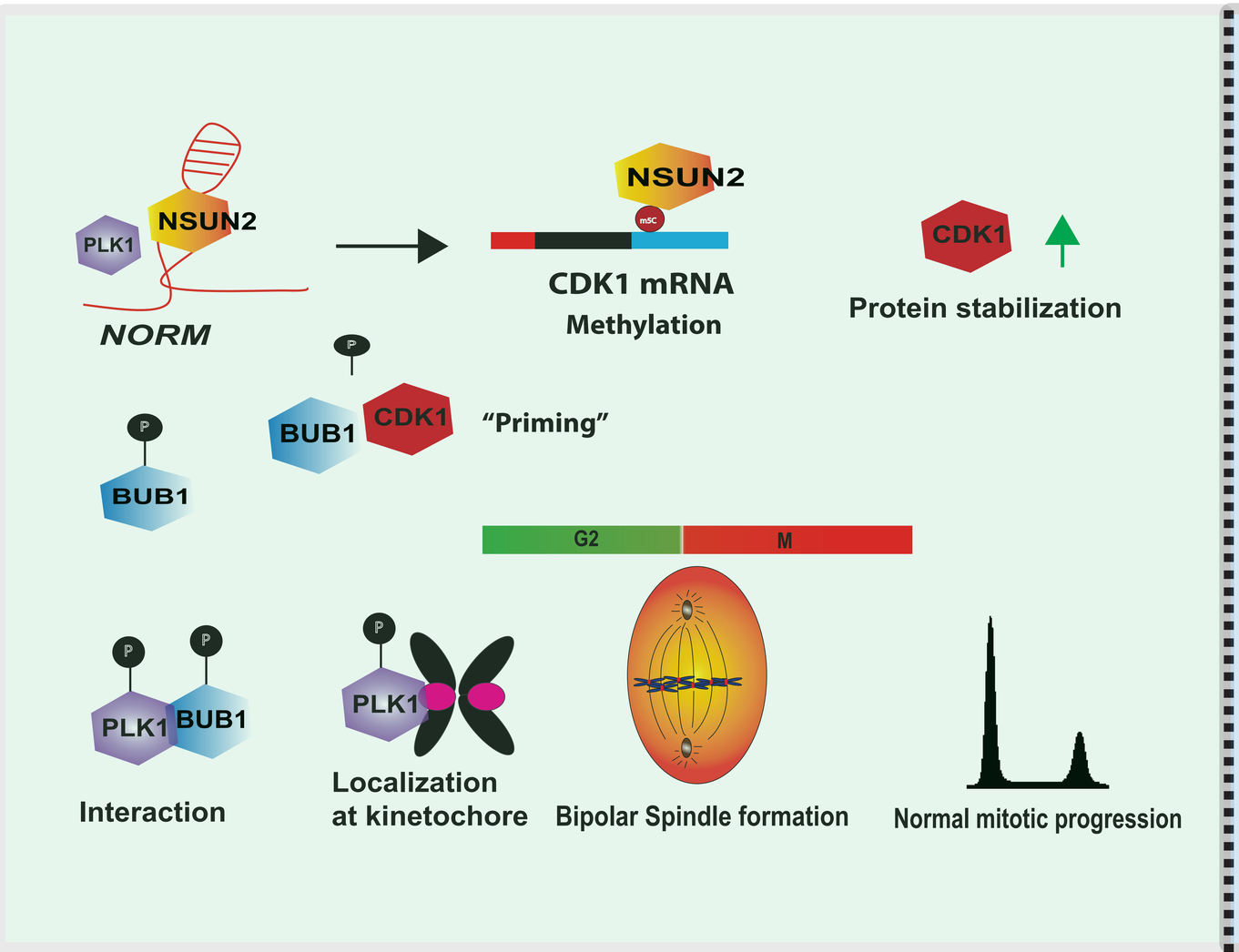
PLK1
NSUN2
NORM
NSUN2
mSC
CDK1 mRNA
Methylation
CDK1
Protein stabilization
P
BUB1
CDK1
"Priming"
P
BUB1
G2
M
P
P
PLK1
BUB1
Interaction
P
PLK1
Localization
at kinetochore
Bipolar Spindle formation
Normal mitotic progression

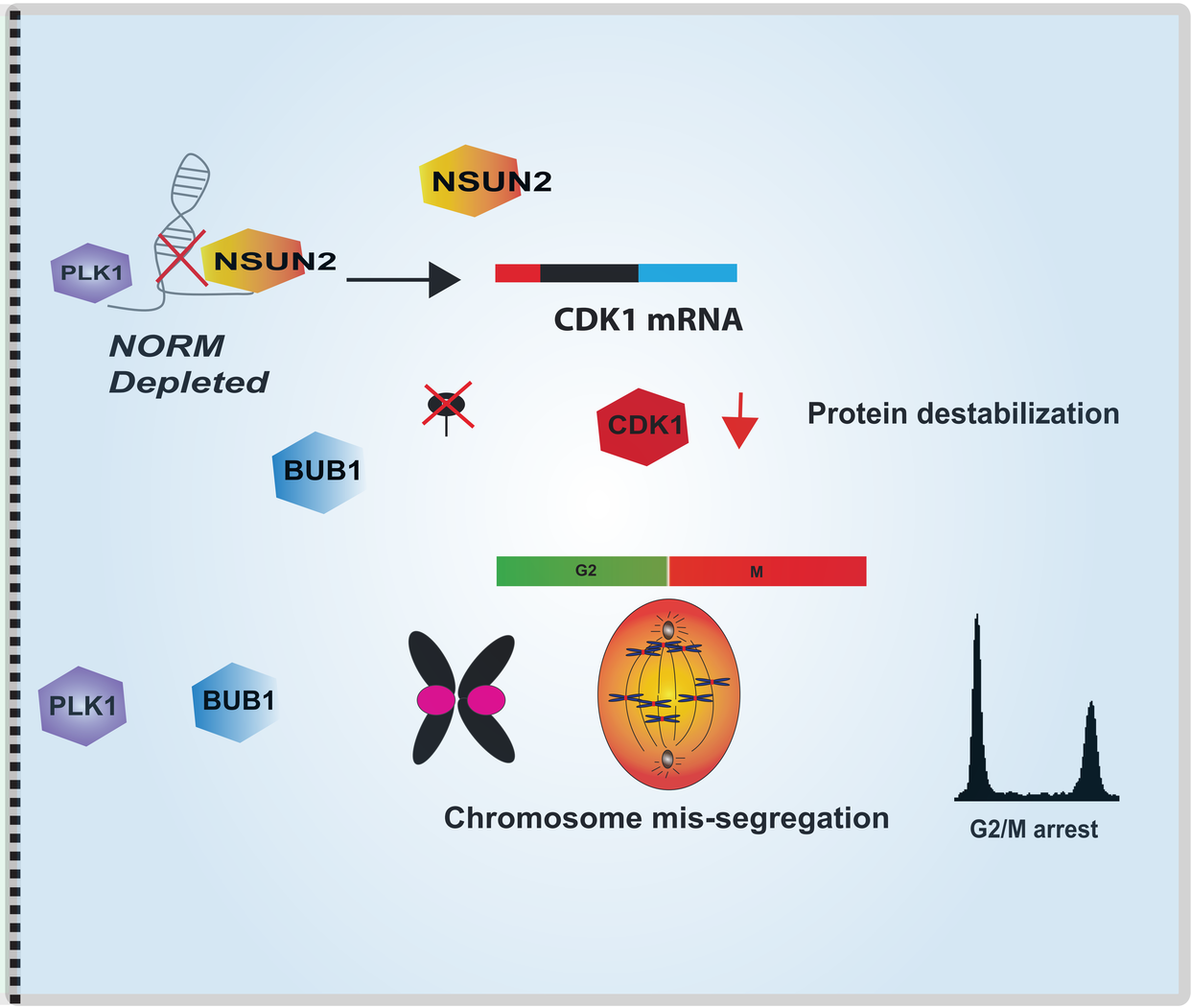
PLK1
NSUN2
NORM
Depleted
NSUN2
CDK1 mRNA
BUB1
CDK1
Protein destabilization
G2
M
PLK1
BUB1
Chromosome mis-segregation
G2/M arrest